metals

MDPI

Article

Residual Stress Evolution during Slot Milling for Repair Welding and Wire Arc Additive Manufacturing of High-Strength Steel Components

Karsten Wandtke [1,*], Amadeus Becker [1], Dirk Schroepfer [1], Arne Kromm [1], Thomas Kannengiesser [1], Ronny Scharf-Wildenhain [2], André Haelsig [2] and Jonas Hensel [2]

[1] Bundesanstalt fuer Materialforschung und -pruefung (BAM), D-12205 Berlin, Germany
[2] Welding Technology, Chemnitz University of Technology, D-09107 Chemnitz, Germany
* Correspondence: karsten.wandtke@bam.de

Abstract: High-strength steels offer potential for weight optimization due to reduced wall thicknesses in modern constructions. Additive manufacturing processes such as Wire Arc Additive Manufacturing (WAAM) enable the resource-efficient production of structures. In the case of defects occurring in weld seams or WAAM components due to unstable process conditions, the economical solution is local gouging or machining and repair welding. It is important to understand the effects of machining steps on the multiaxial stress state in conjunction with the design-related shrinkage restraints. Research into how welding and slot milling of welds and WAAM structures affects residual stresses is still lacking. For this reason, component-related investigations with high-strength steels with yield strengths ≥790 MPa are carried out in our research. In-situ digital image correlation (DIC) and ex-situ X-ray diffraction (XRD) were used to analyze the stresses and strains induced on specimens during and after milling. The systematic analyses revealed a significant interaction of the stiffness and microstructure of the specimens with the initial residual stresses induced by welding. Subsequent repair welds can result in significantly higher residual stresses.

Keywords: high-strength steels; WAAM; residual stress; repair-welding; digital image correlation

Citation: Wandtke, K.; Becker, A.; Schroepfer, D.; Kromm, A.; Kannengiesser, T.; Scharf-Wildenhain, R.; Haelsig, A.; Hensel, J. Residual Stress Evolution during Slot Milling for Repair Welding and Wire Arc Additive Manufacturing of High-Strength Steel Components. *Metals* **2024**, *14*, 82. https://doi.org/10.3390/met14010082

Academic Editor: Kazuyuki Hokamoto

Received: 29 September 2023
Revised: 21 December 2023
Accepted: 26 December 2023
Published: 10 January 2024

1. Introduction

Today, high-strength steels offer the opportunity of meeting high load-bearing requirements in modern steel construction by weight optimizing due to reduced wall thicknesses [1,2]. Additive manufacturing processes such as direct energy deposition using an electric arc (DED-arc [3]) as well as Wire Arc Additive Manufacturing (WAAM) additionally enables direct processing of these steels towards lightweight design geometries and near-net-shape structures providing sustainable and resource-efficient components [4–6]. Furthermore, special welding wires to produce high-strength components using WAAM, developed on the base of high-strength filler materials for joint welding, are already commercially available. The manufacturing of steel structures may introduce unacceptable defects in the weld area or WAAM component, e.g., due to unstable process conditions. In most cases, the economical solution is local gouging or machining of the affected areas and repair welding. Regarding the special microstructure of high-strength steels, a thermal loading may lead to undesirable hardening and degradation of the mechanical properties and should be avoided [7]. Furthermore, the residual stresses on the top layer are influenced by the cooling conditions. In larger welding volumes, cooling and transformation are inhomogeneous in terms of time and location. Thus, the near-surface transverse residual stresses are strongly dependent on the dominant effect (shrinkage, transformation or quenching) [8]. Moreover, investigations in [9] and [10] have shown that the residual stresses in additive manufactured WAAM walls are significantly higher in the welding direction than the residual stresses in the build-up or wall thickness direction.

An appropriate method is machining in terms of slot milling for steel grades with high yield strength, e.g., in mobile crane construction. Therefore, it is necessary to clarify the effects of machining steps on the multi-axial stress state of the welded structure [11]. The mechanical stresses during the repair welding of the groove, which are crucial regarding the limited ductility of high-strength steels, should be considered due to the high shrinkage restraints of the joint groove.

Experimental and simulative studies have shown that reheating instead of welding at an increased preheating temperature with high shrinkage restraint can have a significantly more favorable effect on the resulting residual stress level [12,13]. Thermal gouging causes high heating and cooling rates and significant ductility and toughness losses, especially in multi-pass welds in the areas of the heat-affected zone (HAZ) that are repeatedly heated to temperatures between Ac1 and Ac3 [14]. The resulting short cooling times usually cause martensite formation and unacceptable hardening of the microstructure at the cutting edge. In addition, graphite electrodes lead to carbon enrichment at the joint flanks, which, according to [15], amounts to up to 2% in the cut edges. This leads to a significant change in the morphology of the microstructure in the weld seam and HAZ for the C-enriched areas during welding due to the subsequent repair welding combined with a mixing of the weld metal. Studies show that an increase in the stress level, particularly in the HAZ, occurs with each repair cycle [7].

In this context, component-related investigations in two research projects focus on residual stress affected by welding and machining production steps, such as subsequent machining or local weld seam repair by means of slotting of welds or AM structures, respectively, of steels with yield strength $\geq$790 MPa. Hence, self-restrained geometries of a slot-specimen were identified by means of structural restraint analyses, which cause high welding stresses due to increased design-related shrinkage restraint [16]. In-situ digital image correlation (DIC) and ex-situ X-ray diffraction methods (XRD) enable correlations of the occurring stresses and strains of self-restrained specimens during and after welding and cooling, cf. [17–20]. These analyses were performed systematically during slot milling and revealed a significant interaction between stiffness and relaxation with the initial residual stresses induced by welding. Slot milling, described in [21–26] as the slitting method, involves incrementally cutting a slot into the depth of the specimens, is used to determine the effects on the residual stresses and strains. The analysis of incremental slot milling of the abovementioned high-strength steel welded structures forms the basis for further investigations of the welding- and design-induced stresses during repair welding and machining of AM structures. The aim is to derive recommendations for crack-proof manufacturing and suitable repair concepts of high-strength structural steels for a sustainable and efficient production of lightweight components.

2. Experimental

To determine the influence of milling operations, such as repair welding of a steel structure or the reworking of additively manufactured (AM) components, on the residual stresses, investigations were carried out on a 5-axis DMU 65 machining center (by DMG MORI). The experimental setups for the slot specimen and the AM wall are shown in Figure 1. With a digital image correlation system (DIC), a 3-dimensional measurement was carried out after each milling step to determine the occurring strains and displacements. For this purpose, the samples were prepared with a stochastic pattern as depicted in Figure 1.

The chemical composition of the S960QL base and G 89 filler material for the slot specimen (Figure 1a) is shown in Table 1. The dimensions of the sample are 500 $\times$ 450 $\times$ 20 mm^3 (length $\times$ width $\times$ thickness). The 200 mm long weld seam in the center of the sample was welded with the parameters from Table 2. Due to the slot specimen geometry, a restraint intensity transverse to the weld of R_{Fy} = 11 kN/(mm mm) was realized to simulate the restraint conditions of real component welds [17]. The component used in the study was manufactured with parameters that are suitable for the application, cf. Table 2. The energy per unit length and the $\Delta t_{8/5}$ cooling times are of crucial importance for achieving the

desired mechanical properties. These were selected and fulfilled in accordance with the manufacturer's specifications. As reference, an additional specimen (300 × 220 × 20 mm^3) was welded without shrinkage restraint.

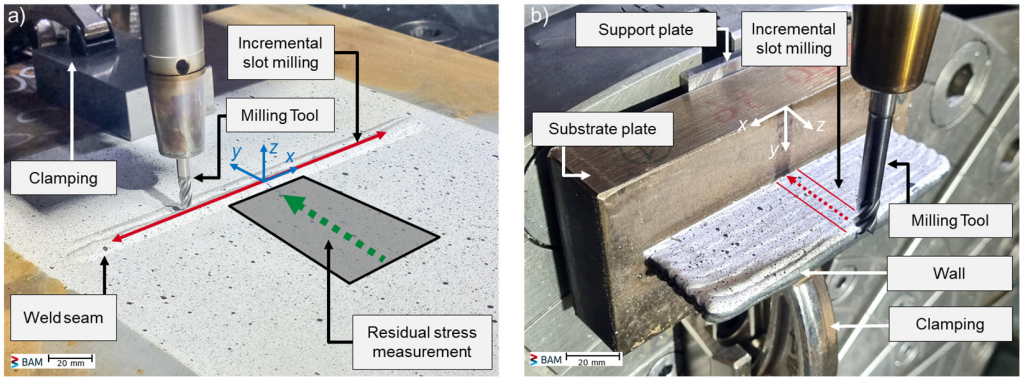

Figure 1. Experimental setup: (**a**) the slot specimen and (**b**) the AM wall.

Table 1. Chemical composition and mechanical properties of base and filler material in wt.-% (OES, Fe: balance).

Base/Filler Metal	C	Si	Mn	Cr	Mo	Ni	$R_{p0.2}$	R_m	A_5
S960QL	0.16	0.21	1.18	0.20	0.58	0.05	1006	1053	17
G 89 6 M21 Mn4Ni2CrMo	0.11	0.81	1.80	0.45	0.57	2.24	1040	1108	15

Table 2. Welding parameters of the slot specimen.

Welding Current/Voltage	Welding Speed	Preheat/Interpass Temperature	Heat Input	$\Delta t_{8/5}$ Cooling Time
222 A/23.1 V	240 mm/min	100 °C/100 °C	1.3 kJ/mm	8.5 s

A ball end milling cutter with a diameter of 6 mm and 4 flutes was used to make a 170 mm long and 11 mm deep slot; the feed of each step was 0.5 mm. In order to simulate a practical machining process, the milling parameters were selected in accordance with the manufacturer's recommendations for the base metal. The parameters in the manufacturer's window were selected to reduce the process forces to a minimum. The ball end milling cutter was used to prevent plastic deformation on edges with small radii. The specimen was clamped in the rear area to allow free expansion in the front where the stochastic pattern is located, and the DIC images were taken.

For the AM wall, a high-strength filler metal specially developed for WAAM with a diameter of 1.2 mm was used. Compared to conventional high-strength solid wire filler materials with a yield strength of at least 790 MPa, e.g., G 79 5 M21 Mn4Ni1.5CrMo (DIN EN ISO 16834) [27], the modification of the alloy composition for WAAM welding enables optimized deposition conditions for layered build-up technologies. Regarding the welding heat control, this ensures an extended processing parameter and operation range and at the same time ensures the required mechanical properties. Table 3 shows the chemical composition and the mechanical properties of the investigated filler metal. A 30 mm thick plate of high-strength steel S690QL with a minimum yield strength of 690 MPa served as the substrate plate. According to the recommendations of the steel producers, this allows welding in a similar working range with regard to heat control for substrate and filler material and, thus, an adequate joining of the AM component. In this way, sufficient ductility in the transition area and, at the same time, sufficiently high strength of the substrate in connection with high stiffness ratios close to the application are realized when welding the components.

Table 3. Chemical composition of the filler metal for the AM wall in wt.-% (OES, Fe: balance).

C	Si	Mn	Cr	Ni	Mo
0.12	0.40	1.91	0.36	2.21	0.61

The AM wall was manufactured from 14 welded layers with a length of 120 mm, a height of 37 mm, and a wall thickness of 11 mm, cf. Table 4. The experimental setup for manufacturing the slot is shown in Figure 1b. The slot was manufactured incrementally from the top of the wall with an infeed of 1 mm per step using a milling cutter with a diameter of 8 mm. At each step, the feed to produce the slot was in the direction of the axis of rotation to ensure a sufficiently large radius, avoiding high notch stresses and plasticizing. The substrate plate was clamped in such a way onto a support plate that the deformation is unrestrained.

Table 4. Welding parameters for the WAAM process.

Welding Gas	Wire Feed	Energy Per Unit Length	Wire Diameter	Interlayer Temperature
97.5% Ar, 2.5% CO_2	4.0 m/min	425 kJ/m	1.2 mm	200 °C

2.1. Digital Imaging Correlation

Two cameras, two lighting devices, a tripod, and a computer with corresponding analysis software (Aramis 6.3 (GOM GmbH, Braunschweig, Germany)) were used to carry out the experiments on digital image correlation (DIC). The lenses used had a focal length of 50 mm, with the cameras positioned at an angle of approximately 27° to each other and a measurement distance of 1.10 m from the measurement area (ARAMIS 3D 4M (GOM GmbH)). The camera system was placed in front of the milling machine to carry out the analyses. After completion of the machining step, the component was moved into the measuring position using a rotary tilting table with a repeat accuracy of 0.01 mm. Before starting the DIC recordings, the components were carefully cleaned of any adhering chips. The presence of adhering chips could have affected the measurements, as they would change the pattern and, thus, influence the accuracy of the results. In addition, the temperature of the components was checked, as they had heated up due to the previous milling process. Due to the thermal expansion of the respective component, it was necessary to carry out the DIC recordings at constant temperatures to ensure reliable and consistent results.

2.2. Residual Stresses Analysis

The residual stresses were analyzed with X-ray diffraction (XRD) using a Goniometer G3 (by Stresstech (Rennerod, Germany)) applying the $\sin^2\psi$ method [28], cf. Table 5. At defined positions, the residual stress was determined transverse to the weld seams on the slot and free shrinking specimens and in the welding direction on the top layer of the AM wall. These measurements were carried out before and after the milling process.

Table 5. Parameters for XRD residual stress analysis.

Measuring Mode	Radiation	Detector	Diffraction Line	2Θ Angle
$\sin^2\psi$	Cr-Kα	Linear solid-state	(211)	156.4°
Collimator Ø	**Tube power**	**ψ–tilting**	**ψ-step**	**Exposure time**
2 mm	30 kV/6.7 mA	0° to ± 45°	10	5 s

2.3. Coordinate Measurement

Tactile coordinate measurement was used to analyze the distortion of the substrate plate in the z-direction. For this purpose, the geometry of the substrate plate was measured along a line in the x-direction before and after machining the AM structure. The line was positioned symmetrically between the AM structure and the edge of the substrate plate in the y-direction. The distance between the start and end points and the edge of the substrate plate in the x-direction was 5 mm. The measuring distance between the points along this line was 2 mm, with the repeatability of the Werth Scope Check S (Werth Messtechnik GmbH (Giessen, Germany)) used being at least 4 µm.

2.4. Hardness Measurement

The analyses of the hardness in the weld seam and base metal were carried out by means of surface hardness measurements on cross-section specimens with the UCI (Ultrasonic contact impedance) method (ISO 50159-1 [29]). The hardness indents were performed out on ground, polished, and etched samples. The hardness was determined with a hardness scanner UT-200 from BAQ GmbH (Braunschweig, Germany). The loading force was 4.903 N (HV 0.5), whereby the indentations were set with a distance to each other of Δs = 0.2 mm and with a duration time of 0.5 s.

3. Results

Figure 2 shows the transverse residual stress profiles $\sigma_y^{rs}(y)$ of the slot specimens in the weld seam, heat affected zone (HAZ), and base material. Maximum stresses are present in the weld metal. The residual stress distribution in the weld zones is the result of a local superposition of restraint shrinkage, quenching, and transformation effects, which leads to typically local maxima in the stress profile on the weld seam and HAZ [18,30]. The comparison between the specimens welded without external restraint (cf. Figure 2a) and welded under restraint in transverse direction (R_{Fy} = 11 kN/(mm mm), cf. Figure 2b) exhibits a significant increase in the transverse residual stresses due to the superposition of global welding stresses (reaction stresses) [11]. Note that the slot specimens were sand blasted before welding, which results in compressive residual stresses of approx. −100 MPa. Hence, an increase in the HAZ of up to 150 MPa is indicated. Maximum transverse residual stresses are to be found in the weld seam of the restraint specimen (cf. Figure 2b) of up to approx. 650 MPa corresponding to over 65% of the nominal yield strength of the material. In the unrestrained specimen, the residual stress decreases to the initial residual stress level (0 MPa) towards the base material at approx. $y = \pm 40$ mm (cf. Figure 2a). The restrained specimen exhibits residual stresses of approx. 150 MPa above the initial stress level of the sand blasted surface at the HAZ, respectively of approx. 100 MPa in the base material ($y = \pm 60$ mm, cf. Figure 2b). After the slot milling of half of the weld metal (in the range from $y = -12$ mm to 0 mm), no significant reduction of the stress profile in the adjacent remaining weld metal was to be found. It can be assumed that this is due to the slot depth of just 10 mm, corresponding to 50% of the plate thickness, which leads to a minor redistribution of the residual stresses in the weld. However, the stress level of the HAZ and base material shows a reduced level of transverse residual stresses by approx. −50 MPa.

For each step of slot milling, DIC analysis was performed (cf. Figure 3a). To determine the effect on the strains of the surface adjacent to the slot, the difference of the distance between a line approx. 20 mm adjacent to the weld seam and a line with a distance of approx. 100 mm was analyzed for each milling step. For this purpose, the strain between six pairs of points was analyzed. The points were positioned on the line near the weld seam and on the line at a distance of 100 mm from the weld seam (cf. Figure 3a). Figure 3b shows the strain as a result of this measurement vs. the slot depth, as well as a polynomial trend line. A positive strain due to slotting corresponds to a reduction in compressive stress and a negative strain to a reduction in tensile stresses in the weld that were analyzed.

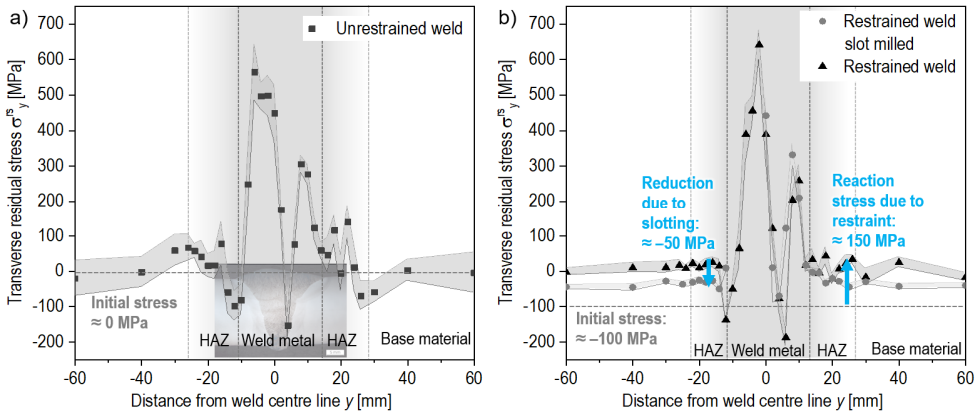

Figure 2. Transverse residual stress profiles $\sigma_y{}^{rs}$ (y) of (**a**) unrestrained welded specimen and (**b**) restrained welded specimen before and after milling.

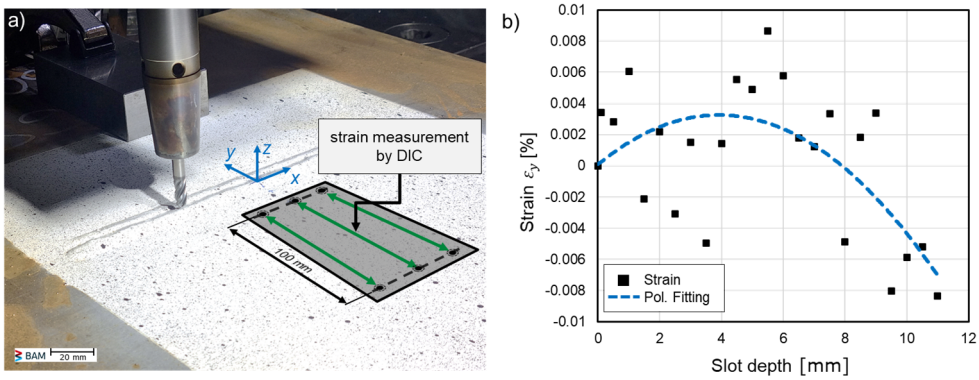

Figure 3. (**a**) Slot specimen with the measurement area and (**b**) strain in *y*-direction vs. slot depth (including weld seam elevation of approx. 3 mm) measured by DIC.

The high deviation of the determined strain for each slotting step results from the measuring arrangement and the low values of the released strains due to slot milling. The analyzed strain and displacement values (in this measurement configuration) are in the range of the measurement resolution and are caused by the interaction of the different microstructures presented in Figure 4. However, the polynomial trend line shows a tendency to expect higher negative strains and thus, a further reduction in transverse tensile residual stresses with further slitting exceeding the neutral axis of the specimen. Hence, it may be concluded that the residual stresses have not relaxed completely, but to a rather small extent due to the insertion of the slot with a depth of 50% of the plate thickness, which is also confirmed by the residual stress analysis (cf. Figure 2b).

The analyzed displacement in the z-direction of the base material is presented in Figure 4. The experimental setup, as shown in Figure 4a, included the evaluation of three measurement points positioned centrally and 200 mm away from the weld. The location and geometry of the slot relative to the weld seam is illustrated, in addition to the hardness mapping, in Figure 4b. Furthermore, three zones are marked in color, which schematically illustrate the local residual stresses in the inhomogeneous microstructure. Figure 4c depicts the diagram of the analyzed displacement w_z vs. the slot depth. In conclusion, the results and the resulting effects are shown schematically in Figure 4d. Figure 4b reveals that the slot was manufactured in the area where the last bead was welded. Due to the material, the cooling rate, and the lack of subsequent layers, a typical hardness profile of a multi-layer weld seam can be seen. The used filler metal transforms into martensitic at high cooling rates. This solid phase transformation causes compressive residual stresses in the volume in the area of increased hardness and residual tensile stresses in the tempered material beneath.

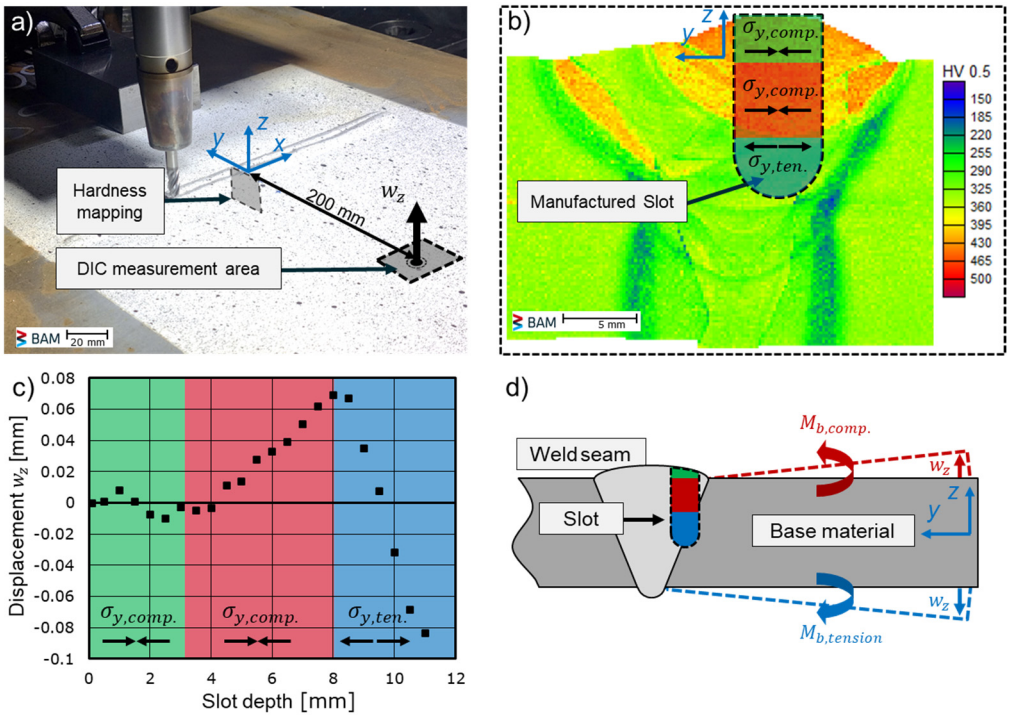

Figure 4. (**a**) Slot specimen with the measurement area; (**b**) hardness map with schematic slot and residual stresses; (**c**) displacement in *z*-direction vs. slot depth measured by DIC; and (**d**) schematic illustration of the distortion of the component.

The deformation in the base metal is caused by the interaction between the local residual stresses, the milling process, and the resulting relaxation of the residual stresses due to the inhomogeneous microstructure. The analyzed displacement w_z of the base material vs. slot depth is presented in Figure 4c. The results indicate the different behavior of the microstructure at different slot depths (cf. Figure 4b); three zones were identified. In the first zone, which is marked in green in Figure 4c, the displacement w_z shows no significant change with increasing slot depth, even though a higher hardness was analyzed (cf. Figure 4c). However, when the level of the base metal is reached (cf. Figure 4b), a significant change in the displacement w_z is observed. The base metal shifts significantly in the positive *z*-direction with increasing slot depth (red marking). In the area of high hardness, the residual compressive stress associated with the solid phase transformation is relaxed in the y-direction (see Figure 4d). With further machining and increasing slot depth (marked in blue), the residual tensile stress present in the tempered area of the weld seam relaxes. The base material shifts in the negative z-direction. Due to the structural rigidity of the component, the influence on the residual stresses near the surface was significantly reduced, so only minor residual stress changes and strains could be analyzed. In the case of repair welding, as was exemplarily considered, this would, hence, introduce further welding stresses into the weld and surrounding area, which could increase the risk of cracking.

Figure 5a presents the AM wall after slot milling, as well as the area for determining the residual stress σ_x^{rs} (Figure 5b), the displacement Δz (Figure 5c), and the strain ε_x across the slot (Figure 5d). The residual stresses were analyzed on the top layer of the AM wall in the welding direction (*x*-direction) at five measurement points with a defined distance of 10 mm (cf. Figure 5b). The residual stresses at the positions x = 15 mm to x = 35 mm are approx. 250 MPa and increase to 480 MPa towards the edge. As a result of the slot and release of the restraint of the structure, the residual stresses decrease or redistribute by approx. 30–40%. The displacement of the substrate plate Δz was determined in the as-welded state and after milling. The measurement area was parallel to the wall (Figure 5a). Figure 5c presents the measured displacement $\Delta z(x)$ on the substrate plate. A maximum

displacement of Δz = –0.24 mm was previously measured in the center of the substrate plate as a consequence of welding, which decreased by 50% to $\Delta z = -0.12$ mm after milling the slot.

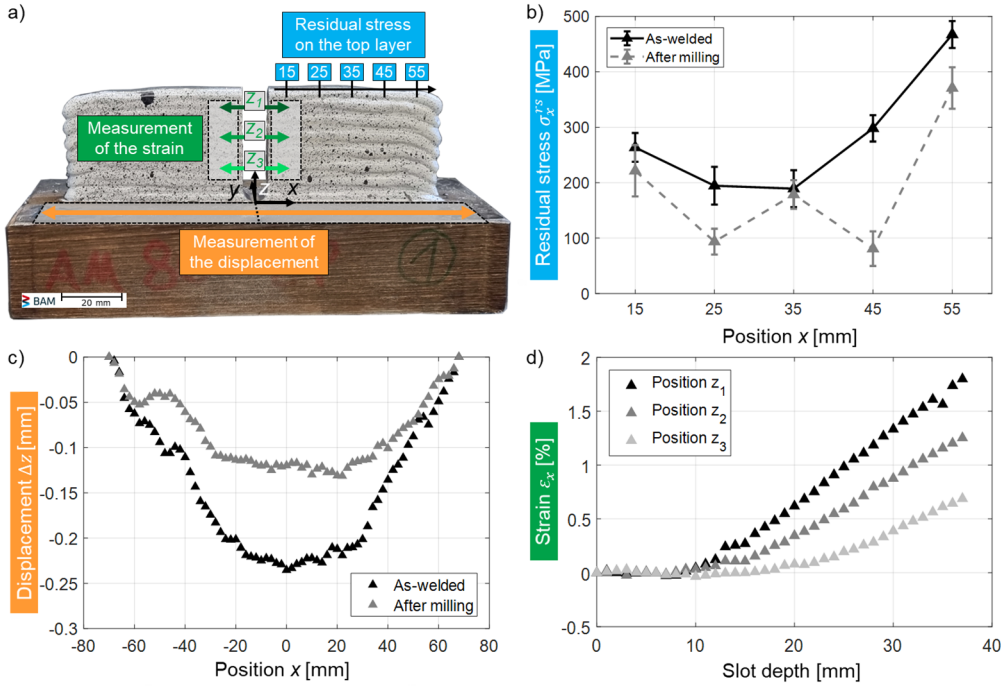

Figure 5. (**a**) AM wall with the measurement areas; (**b**) residual stress $\sigma_x^{rs}(x)$ on the top layer (XRD); (**c**) measured displacement in z-direction; and (**d**) strain across the slot (DIC).

Figure 5d presents the strain of the AM wall versus the slot depth. The difference in the distances between pairs of points in the measurement areas at heights z_1 = 32 mm z_2 = 20 mm and z_3 = 8 mm, which have equidistant distances to each other and are not directly at the boundary of the component in order to avoid boundary effects, was determined. A considerable effect on the strain is exhibited at a slot depth of 9 mm, which is assumably due to the release of the restraint of the structure. Moreover, microstructure investigations showed higher hardness and divergent microstructure for the last three weld layers of this filler material. The significantly higher hardness resulted from the lack of repeated annealing of the layers by subsequent weld beads [31]. Thus, it is assumed that the divergent microstructure of the top layers affects the residual stress distribution due to the predominant effects of a solid phase transformation in connection with a restrained volume expansion [30,32,33], primarily in longitudinal direction at the top 9 mm of the wall, causing a lower displacement due to slotting. Beyond reaching a slot depth of 22 mm, the strain increases almost linearly at each step, which is related to the displacement of the substrate plate. It is intended to provide further information on this in subsequent investigations of the residual stresses in the bulk of the specimen.

4. Summary

Investigations were carried out to identify the influence of machining on a welded slot specimen and an additively manufactured specimen on the welding-induced residual stresses and the resulting distortions. The following results were obtained:

(1) Digital image correlation, X-ray diffraction, and coordinate measurement were used to analyze the influence of milling on the slot specimen and the AM wall structure.
(2) Slot milling of a welded self-restrained slot specimen for a repair preparation reveals only a significant effect by a reduction of approx. 30% in the transverse residual stress level in the HAZ and base material surrounding the weld seam and no effect on the weld metal.

(3) The released strains due to slotting perpendicular to the weld are rather small, with a trend of become greater with increasing slotting depth above 50% of the plate thickness (exceeding the neutral axis). Therefore, it can be assumed that a repair weld of the milled slot would introduce increased welding stresses into the weld and the surrounding area, which would be detrimental to the component performance and crack safety during production and service.
(4) The displacement of the base material in the z-direction due to the milling process is significantly determined by the inhomogeneous microstructure. The relaxation of the residual stresses during machining causes the component to deform in the vertical direction. This displacement occurs in opposing directions. In the area of high hardness, the residual compressive stress causes a shift in the positive z-direction. In the area of tempered material, the tensile residual stress caused a shift in the negative z-direction.
(5) The residual stresses on the top layer of the AM wall segment were reduced by an average of 30–40% by slot milling in the center axis.
(6) The angular distortion of the substrate plate is reduced by 50% due to the milling of the slot. The resulting decrease in distortion is in good correlation with the analyzed residual stress relief. This shows that in the AM wall, tensile residual stresses occur predominantly in the longitudinal direction, the direction with the most severe shrinkage restraint.
(7) The strain as a function of slot depth shows no significant increase up to a depth of 9 mm, which is assumed to be the result of a divergent microstructure. Beyond a slot depth of 22 mm, the strain shows a linear progression, presumably resulting from the displacement of the substrate plate.

The study investigated the material S960 and a modified G 89 filler metal. The results presented show the influence of slot milling on the formation of residual stresses in high-strength steel components and serve as a basis for further investigations. DIC analyses provide a three-dimensional way of recording the strains and displacements and, thus, the reactions of the component to machining steps. However, during milling, the DIC is mainly influenced by the chips from the milling process and the deposition of chips on the sample as well as the temperature and the associated thermal expansion. Careful removal of the chips and recording the data at the same temperatures is therefore crucial for reliable data. In further planned investigations, the influence of other steel grades, modified self-restraint properties, and the influence of seam preparation on the residual stresses at butt joints will be examined. In addition, the influence of processing the top layer and finishing milling on the distortion of AM structures will be investigated. The objective of these investigations is to develop recommendations for the handling and processing for repair welding and stress-optimized joining of high-strength steels.

Author Contributions: Conceptualization, K.W., A.B. and D.S.; methodology, K.W., A.B., D.S. and A.K.; formal analysis, K.W., A.B. and D.S.; investigation, K.W. and A.B.; resources, D.S., T.K., R.S.-W., A.H. and J.H.; writing—original draft preparation, K.W., D.S., A.K., R.S.-W. and A.H.; writing—review and editing, K.W., A.B., D.S., A.K., T.K., R.S.-W., A.H. and J.H.; visualization, K.W. and D.S.; supervision, D.S., T.K., A.H., and J.H.; project administration, D.S., T.K., A.H. and J.H. All authors have read and agreed to the published version of the manuscript.

Funding: The IGF project No. 20162 N (P 1311) and No. 21162 BG (P 1380) of the Research Association for Steel Application (FOSTA) was funded by the Federal Ministry for Economic Affairs and Climate Action via the German Federation of Industrial Research Associations (AiF) as part of the program for the promotion of the Industrial Collective Research (IGF) on the basis of a resolution of the German Bundestag. We would like to express gratitude for this funding, as well as for the cooperation and support of the companies and persons actively involved in the project advisory committee. We also thank Andreas Boerner from the BAM for his support in the milling experiments.

Data Availability Statement: The data presented in this study are available on request from the corresponding author. The data are not publicly available due to restrictions since the research is ongoing at the moment.

Conflicts of Interest: The authors declare no conflict of interest.

References

1. Günther, H.-P.; Raoul, J. *Use and Application of High-Performance Steels for Steel Structures*; IABSE: Zürich, Switzerland, 2005; Available online: http://app.knovel.com/hotlink/toc/id:kpUAHPSSS1/use-and-application (accessed on 24 August 2023).
2. Hulka, K.; Kern, A.; Schriever, U. Application of Niobium in Quenched and Tempered High-Strength Steels. *Mater. Sci. Forum* **2005**, *500–501*, 519–526. [CrossRef]
3. *ISO/ASTM 52900*; Additive Manufacturing—General Principles—Terminology. Beuth: Berlin, Germany, 2015.
4. Frazier, W.E. Metal Additive Manufacturing: A Review. *J. Mater. Eng. Perform.* **2014**, *23*, 1917–1928. [CrossRef]
5. Plangger, J.; Schabhüttl, P.; Vuherer, T.; Enzinger, N. CMT Additive Manufacturing of a High Strength Steel Alloy for Application in Crane Construction. *Metals* **2019**, *9*, 650. [CrossRef]
6. Treutler, K.; Wesling, V. The Current State of Research of Wire Arc Additive Manufacturing (WAAM): A Review. *Appl. Sci.* **2021**, *11*, 8619. [CrossRef]
7. Schasse, R.; Kannengiesser, T.; Kromm, A.; Mente, T. Residual stresses in repair welds of high-strength low-alloy steels. *Weld. World* **2015**, *59*, 757–765. [CrossRef]
8. Christian, H.; Elfinger, F.-X. Eigenspannungen in Schweißnähten. *Der Maschinenschaden* **1978**, *51*, 124–130.
9. Wu, Q.; Mukherjee, T.; De, A.; DebRoy, T. Residual stresses in wire-arc additive manufacturing—Hierarchy of influential variables. *Addit. Manuf.* **2020**, *35*, 101355. [CrossRef]
10. Ding, J.; Colegrove, P.; Mehnen, J.; Ganguly, S.; Sequeira Almeida, P.M.; Wang, F.; Williams, S. Thermo-mechanical analysis of Wire and Arc Additive Layer Manufacturing process on large multi-layer parts. *Comput. Mater. Sci.* **2011**, *50*, 3315–3322. [CrossRef]
11. Schroepfer, D.; Kromm, A.; Schaupp, T.; Kannengiesser, T. Welding stress control in high-strength steel components using adapted heat control concepts. *Weld. World* **2019**, *63*, 647–661. [CrossRef]
12. Wongpanya, P. *Effects of Heat Treatment Procedures on the Cold Cracking Behaviour of High Strength Steel Welds*; Bundesanstalt für Materialforschung und -prüfung (BAM): Berlin, Germany, 2008.
13. Wongpanya, P.; Boellinghaus, T.; Kannengiesser, T.; Lothongkum, G. Effects of preheating and interpass temperature on stresses in S 1100 QL multi-pass butt-welds. *Weld. World* **2008**, *52*, 79–92. [CrossRef]
14. Schulze, G. *Die Metallurgie des Schweißens: Eisenwerkstoffe—Nichteisenmetallische Werkstoffe*; Springer: Berlin/Heidelberg, Germany, 2004.
15. Miltyutin, V.S. The effect of arc-air cutting on the quality of metal. *Weld. Prod.* **1979**, *26*, 44–46.
16. Satoh, K.; Ueda, Y.; Kihara, H. Recent trends of research into restraint stresses and strains in relation to weld cracking. *Weld. World* **1973**, *11*, 133–156.
17. Amadeus, B.; Dirk, S.; Arne, K.; Thomas, K. Determination of residual stress evolution during repair welding of high-strength steel components. *Forces Mech.* **2022**, *6*, 100073. [CrossRef]
18. Schroepfer, D.; Kromm, A.; Kannengiesser, T. Load analyses of welded high-strength steel structures using image correlation and diffraction techniques. *Weld. World* **2018**, *62*, 459–469. [CrossRef]
19. Boruah, D.; Dewagtere, N.; Ahmad, B.; Nunes, R.; Tacq, J.; Zhang, X.; Guo, H.; Verlinde, W.; De Waele, W. Digital Image Correlation for Measuring Full-Field Residual Stresses in Wire and Arc Additive Manufactured Components. *Materials* **2023**, *16*, 1972. [CrossRef]
20. Cunha, F.G.; Santos, T.G.; Xavier, J. In Situ Monitoring of Additive Manufacturing Using Digital Image Correlation: A Review. *Materials* **2021**, *14*, 1511. [CrossRef] [PubMed]
21. Tabatabaeian, A.; Ghasemi, A.R.; Shokrieh, M.M.; Marzbanrad, B.; Baraheni, M.; Fotouhi, M. Residual Stress in Engineering Materials: A Review. *Adv. Eng. Mater.* **2022**, *24*, 2100786. [CrossRef]
22. Zhang, Y.; Nelson, D. Residual Stresses in Bone as Determined by a Slotting Method. *Exp. Mech.* **2017**, *57*, 967–978. [CrossRef]
23. Shokrieh, M.M. *Residual Stresses in Composite Materials*; Woodhead Publishing: Oxford, UK, 2021.
24. Olson, M.D.; DeWald, A.T.; Hill, M.R. Measurement Layout for Residual Stress Mapping Using Slitting. *Exp. Mech.* **2022**, *62*, 393–402. [CrossRef]
25. Olson, M.D.; Hill, M.R. Two-Dimensional Mapping of In-plane Residual Stress with Slitting. *Exp. Mech.* **2018**, *58*, 151–166. [CrossRef]
26. Olson, M.D.; Watanabe, B.T.; Wong, T.A.; DeWald, A.T.; Hill, M.R. Near Surface Residual Stress Measurement Using Slotting. *Exp. Mech.* **2022**, *62*, 1401–1410. [CrossRef]
27. *DIN EN ISO 16834*; Welding Consumables–Wire Electrodes, Wires, Rods and Deposits for Gas Shielded Arc Welding of High Strength Steels. Beuth: Berlin; Germany, 2012.
28. Withers, P.J.; Bhadeshia, H.K.D.H. Residual stress. Part 1—Measurement techniques. *Mater. Sci. Technol.* **2001**, *17*, 355–365. [CrossRef]

29. *DIN 50159-1*; Metallic Materials—Hardness Testing with the UCI Method—Part 1: Test Method. Beuth: Berlin, Germany, 2022.
30. Withers, P.J.; Bhadeshia, H.K.D.H. Residual stress. Part 2—Nature and origins. *Mater. Sci. Technol.* **2001**, *17*, 366–375. [CrossRef]
31. Wandtke, K.; Schröpfer, D.; Scharf-Wildenhain, R.; Hälsig, A.; Kromm, A.; Kannengießer, T. WAAM Process Influences on Local Microstructure and Residual Stresses in High-Strength Steels. In Proceedings of the 46th MPA-Seminar Manuscripts, Stuttgart, Germany, 12–13 October 2021; pp. 296–306. Available online: https://opus4.kobv.de/opus4-bam/frontdoor/index/index/docId/53571 (accessed on 28 July 2023).
32. Nitschke-Pagel, T.; Dilger, K. Sources and Consequences of Residual Stresses due to Welding. *Mater. Sci. Forum* **2014**, *783–786*, 2777–2785. [CrossRef]
33. Sun, J.; Nitschke-Pagel, T.; Dilger, K. Generation and distribution mechanism of welding-induced residual stresses. *J. Mater. Res. Technol.* **2023**, *27*, 3936–3954. [CrossRef]